J Biol Inorg Chem (2001) 6:300–314
DOI 10.1007/s007750000204

ORIGINAL ARTICLE

**Francesco Musiani · Elisa Arnofi · Rita Casadio
Stefano Ciurli**

# Structure-based computational study of the catalytic and inhibition mechanisms of urease

Received: 9 October 2000 / Accepted: 17 December 2000 / Published online: 28 February 2001


**Abstract** The viability of different mechanisms of catalysis and inhibition of the nickel-containing enzyme urease was explored using the available high-resolution structures of the enzyme isolated from *Bacillus pasteurii* in the native form and inhibited with several substrates. The structures and charge distribution of urea, its catalytic transition state, and three enzyme inhibitors were calculated using ab initio and density functional theory methods. The DOCK program suite was employed to determine families of structures of urease complexes characterized by docking energy scores indicative of their relative stability according to steric and electrostatic criteria. Adjustment of the parameters used by DOCK, in order to account for the presence of the metal ion in the active site, resulted in the calculation of best energy structures for the nickel-bound inhibitors $\beta$-mercaptoethanol, acetohydroxamic acid, and diamidophosphoric acid. These calculated structures are in good agreement with the experimentally determined structures, and provide hints on the reactivity and mobility of the inhibitors in the active site. The same docking protocol was applied to the substrate urea and its catalytic transition state, in order to shed light onto the possible catalytic steps occurring at the binuclear nickel active site. These calculations suggest that the most viable pathway for urea hydrolysis involve a nucleophilic attack by the bridging, and not the terminal, nickel-bound hydroxide onto a urea molecule, with active site residues playing important roles in orienting and activating the substrate, and stabilizing the catalytic transition state.

**Keywords** Urease · *Bacillus pasteurii* · DOCK program · Nickel · Reaction mechanism

**Abbreviations** *AHA*: acetohydroxamic acid · *BME*: $\beta$-mercaptoethanol · *BPU*: *Bacillus pasteurii* urease · *DAP*: diamidophosphate · *KAU*: *Klebsiella aerogenes* urease · *PPD*: phenylphosphorodiamidate

## Introduction

The rapid hydrolysis of urea catalyzed by the nickel-containing enzyme urease (urea amidohydrolase, E.C. 3.5.1.5) in algae, fungi, and bacteria [1] causes an abrupt increase of pH and, consequently, negative side effects in agriculture [2, 3, 4] and health [2, 5, 6]. The full understanding of the catalytic mechanism of enzymatic urea hydrolysis, as well as the capability to control the rate of this reaction using structure-based designed urease inhibitors, are important goals to pursue. The presence, in urease, of a catalytic binuclear metal center, constituted by two nickel atoms, renders this endeavor particularly challenging. In fact, the influence of the stereoelectronic properties of the open-shell Ni(II) $d^8$ ions on the reactivity of the reaction site is not easy to predict accurately. We present here a novel approach to the solution of this problem, which involves the use of relatively simple and fast calculations that are capable of reproducing the crystallographically determined structures of urease, therefore providing reliable predictions of the reactivity of substrate and transition state in the active site.

The structures of urease from *Klebsiella aerogenes* (KAU) [7] and *Bacillus pasteurii* (BPU) [8] have been determined, revealing an analogous $\alpha_3\beta_3\gamma_3$ quaternary structure and very similar active site geometry [9]. In

F. Musiani · S. Ciurli (✉)
Department of Agro-Environmental Science and Technology, University of Bologna, Viale Berti Pichat 10, 40127 Bologna, Italy
E-mail: sciurli@agrsci.unibo.it
Phone: +39-051-2099794
Fax: +39-051-243362

E. Arnofi · R. Casadio
Laboratory of Biophysics, University of Bologna, Via Irnerio 42, 40126 Bologna, Italy

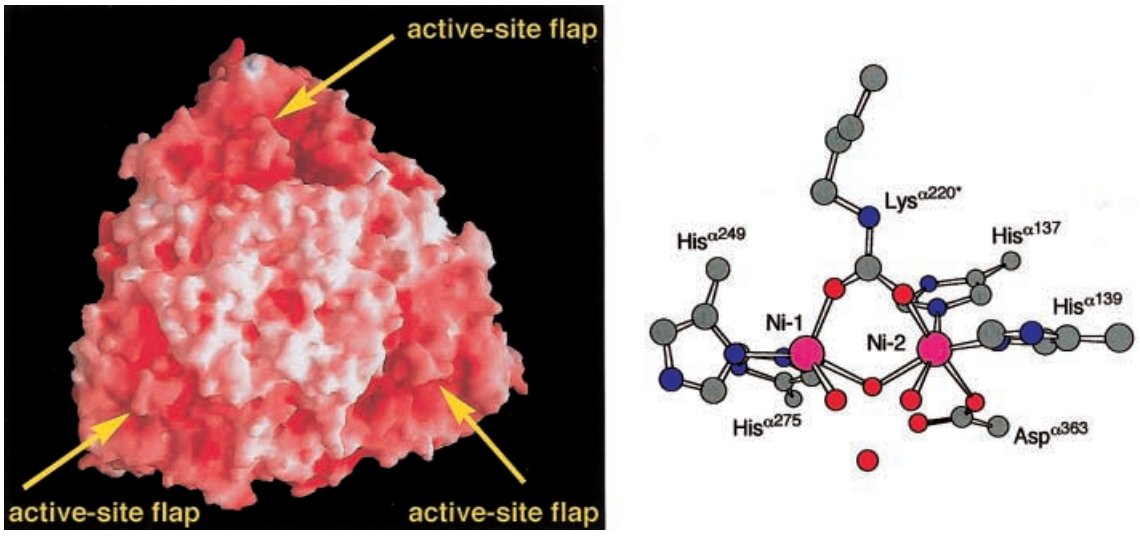


**Fig. 1** Solid surface representation of the electrostatic potential of *B. pasteurii* urease. The molecular surface and electrostatic mapping were generated by the program GRASP [35], using a probe radius of 1.4 Å. The electrostatic potential was calculated using a simple version of a Poisson-Boltzmann solver, with the GRASP full charge set. Dielectric constants of 80 and 2 were used for the solvent and protein interior, respectively. All histidines were considered neutral. The surface is colored according to the calculated electrostatic potential contoured from –27.5 *kT/e* (*intense red*) to +25.8 *kT/e* (*intense blue*). The *right panel* shows the coordination geometry of the active site nickel ions. Atoms are colored according to the following scheme: nickel, *magenta*; carbon, *grey*; nitrogen, *blue*; oxygen, *red*

the structure of native BPU (PDB code 2UBP, resolution 2.0 Å), the active site is found in the $\alpha$-subunit, at the bottom of a ca. 15 Å deep channel characterized by the presence of a negative electrostatic surface (Fig. 1) and by a flexible helix-turn-helix flap. In the structure of native BPU the flap is found in an open conformation, while in native KAU the flap is closed [7], indicating a relative flexibility of this structural motif.

The two nickel ions in the active site of BPU are bridged by the carbamylated Lys$^{\alpha 220*}$ as well as by a hydroxide ion. One Ni ion (Ni(1)) is further coordinated by His$^{\alpha 249}$ N$\delta$ and His$^{\alpha 275}$ N$\varepsilon$, while Ni(2) is bound to His$^{\alpha 137}$ N$\varepsilon$, His$^{\alpha 139}$ N$\varepsilon$, and Asp$^{\alpha 363}$ O$\delta$1. The coordination geometry of each Ni ion is completed by one water molecule (see Fig. 1, and Table 1 for metal-ligand distances).

In the case of BPU, the structural details of the binding of inhibitors such as $\beta$-mercaptoethanol (BME) [10], acetohydroxamic acid (AHA) [11], and phenylphosphorodiamidate (PPD) [8] were also elucidated. In BPU inhibited with BME (PDB code 1UBP, resolution 1.65 Å, Fig. 2A) the sulfur atom of BME symmetrically bridges the binuclear Ni center. BME further chelates Ni(1) using its terminal OH [10], resulting in both Ni ions being pentacoordinate (Table 1). Another molecule of BME forms a mixed disulfide with Cys$^{\alpha 322}$, and its terminal OH group is H-bound to the carbonyl group of Ala$^{\alpha 366}$, fixing the flexible active site flap in the open conformation, as well as sealing, by steric hindrance, the active site entrance.

The structure of BPU inhibited with AHA (PDB code 4UBP, resolution 1.55 Å, Fig. 2B) reveals the binding mode of the inhibitor, symmetrically bridging the two Ni ions in the active site through the hydroxamate oxygen, and chelating Ni(1) through the carbonyl oxygen (Table 1) [11]. The flexible flap flanking the active site cavity is in the open conformation.

**Table 1** Summary of the relevant distances (Å) in the active site of native and inhibited BPU

| Protein<br>PDB code | Native BPU<br>2UBP | DAP-BPU<br>3UBP | BME-BPU<br>1UBP | AHA-BPU<br>4UBP |
|---|---|---|---|---|
| Ni(1)-Ni(2) | 3.7 | 3.8 | 3.1 | 3.5 |
| His$^{\alpha 249}$ N$\delta$-Ni(1) | 2.2 | 2.0 | 2.2 | 2.0 |
| His$^{\alpha 275}$ N$\varepsilon$-Ni(1) | 2.2 | 2.1 | 2.2 | 2.0 |
| Lys$^{\alpha 220*}$ O$\theta$1-Ni(1) | 2.1 | 2.1 | 2.1 | 2.0 |
| AHA $O_B(W_B, S_B)$-Ni(1) | 2.1 | 2.3 | 2.3 | 2.0 |
| AHA $O_T(W_1)$-Ni(1) | 2.2 | 2.2 | 2.3 | 2.2 |
| His$^{\alpha 137}$ N$\varepsilon$-Ni(2) | 2.2 | 2.1 | 2.1 | 2.0 |
| His$^{\alpha 139}$ N$\varepsilon$-Ni(2) | 2.2 | 2.2 | 2.1 | 2.0 |
| Lys$^{\alpha 220*}$ O$\theta$2-Ni(2) | 2.1 | 1.9 | 2.1 | 2.0 |
| Asp$^{\alpha 363}$ O$\delta$1-Ni(2) | 2.2 | 2.1 | 2.1 | 2.1 |
| AHA $O_B(W_B, S_B)$-Ni(2) | 2.2 | 2.3 | 2.3 | 2.0 |

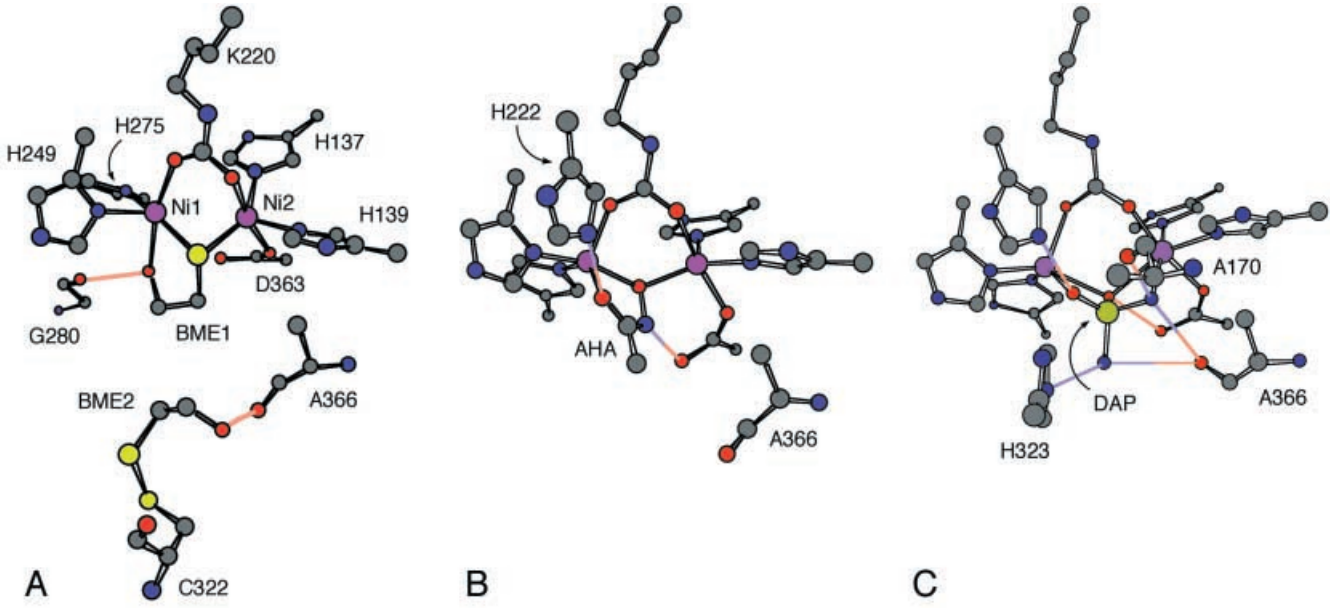


**Fig. 2** Crystal structure of **A** BME-, **B** AHA-, and **C** DAP-inhibited BPU (color scheme: nickel, *magenta*; carbon, *grey*; nitrogen, *blue*; oxygen, *red*; sulfur, *yellow*; phosphorus, *orange*). The proposed H-bonds are colored according to the donor-acceptor scheme

A molecule of diamidophosphoric acid (DAP) is found in the active site of urease crystallized in the presence of the slow, tight-binding inhibitor PPD (PDB code 3UBP, resolution 2.0 Å, Fig. 2C). DAP is the product of the enzymatic hydrolysis of PPD [12] and binds the bimetallic center using three of the four potentially coordinating atoms, in an unprecedented mode. One oxygen atom of DAP replaces the Ni-bridging hydroxide observed in native BPU, one oxygen and one nitrogen atoms bind to Ni(1) and Ni(2), respectively, while the second nitrogen atom of DAP points away, towards the cavity opening [8].

DAP is a transition state analogue, and its mode of binding to the Ni ions suggested a mechanism for enzymatic urea hydrolysis which reconciled the available structural and biochemical data [8, 9]. This mechanism involves a direct role of the Ni bridging hydroxide (shown to be labile by the several cases where it was substituted by an incoming ligand) as the nucleophile in the process of urea hydrolysis. An alternative proposal suggests a hydroxide ion bound to Ni(2) as the nucleophile [13]. These two possible mechanisms are shown in Scheme 1.

In DAP-inhibited BPU the active site flap is found in a closed conformation. Changes in the flap confor-

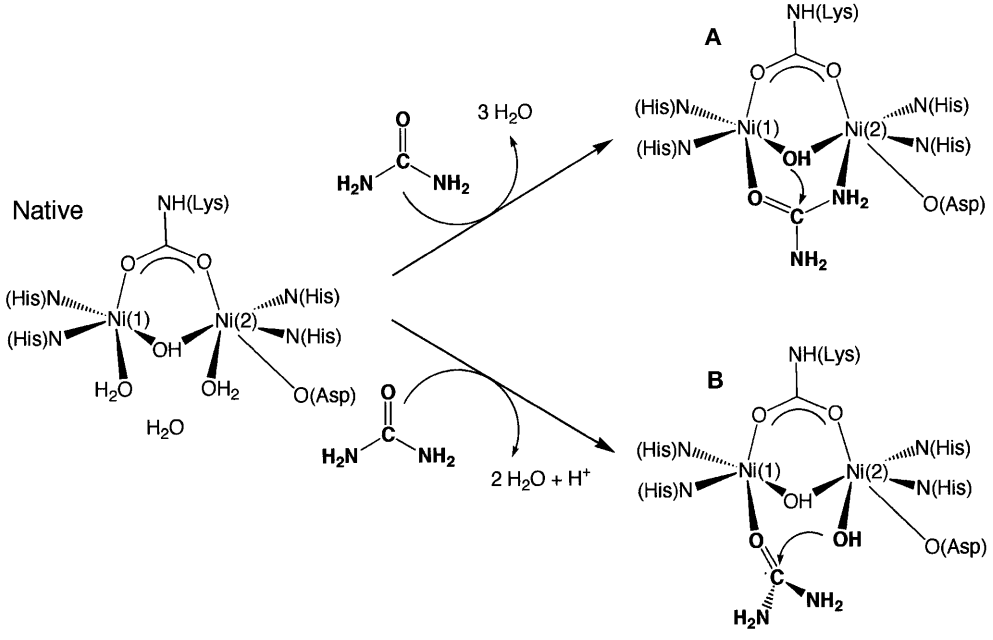


**Scheme 1**

mation, besides determining the accessibility of the active site channel, directly affect the position of important residues such as His$^{\alpha 323}$ and Ala$^{\alpha 366}$ (Fig. 2). His$^{\alpha 323}$, shown to be responsible for the lower p$K_a$ (6.5) of the bell-shaped pH/activity profile [14, 15], is shifted away from the Ni ions when the flap is open. Furthermore, Ala$^{\alpha 366}$ points its carbonyl group toward or away from the Ni ions when the flap is closed or open, respectively. Only when the flap is closed can both these residues be involved in the H-bond network that stabilizes the binding of DAP (and putatively also of the catalytic transition state) to the binuclear Ni center (Fig. 2C) [8, 9].

This report describes how the viability of the two proposed reaction mechanisms for urease, shown in Scheme 1, can be tested using docking algorithms. In particular, the study is aimed at testing the viability of the two proposed mechanisms as far as the substrate binding mode and the nucleophilic attack are concerned. Other steps in the mechanism, such as, for example, the proton transfer to a urea amide group to yield ammonia, will not be addressed.

The docking calculations adopted in this work yield favorable orientations of ligands in a receptor using optimization of steric and electrostatic interactions. In the case of urease, the receptor is constituted by the nickel-containing active site, while the ligands can be substrates, inhibitors, or even short-lived transition states, whose geometric and charge distribution parameters are calculated using ab initio and density functional theory (DFT) methods [16, 17]. In fact, the novelty of the present approach is the docking of transient chemical moieties that cannot be determined otherwise, shedding light on the reaction mechanism. The present study was performed using the program DOCK [18], software utilized to perform docking calculations of small molecules into macromolecular systems. DOCK is more generally used to design possible inhibitors that can be tested as new drugs [19, 20]. Here we want to propose a new use of this algorithm, that is, the exploration of possible reaction paths.

## Materials and methods

### Computational methods

The DOCK 4.0.1 program suite [18, 21, 22, 23] was used. The general computational strategy involves several steps. First, the possible location of positions for ligand atoms within the active site region are calculated as the centers of overlapping spheres of variable radii, which fill up the site. In this way, the shape properties of the active site cavity are determined. Second, an electrostatic potential grid is computed, within the volume defined as above, by taking into account net and partial charges on protein atoms located within a certain cut-off distance from the active site. Finally, the possible orientations of a ligand inside the reaction site, and their relative ligand-receptor interaction energies, are calculated.

### Active site characterization

The molecular surface of the urease receptor cavity was built using Connolly's MS algorithm (QCPE version) [24, 25], using a probe atom with a radius of 1.0 Å [26] and a dot density of 8 points/Å. A radius of 0.83 Å was used for the nickel ions [27]. The program SPHGEN [18] was used to fill the calculated cavity with spheres having variable radii (1.0–4.0 Å). The cavity surface was calculated considering the active site flexible flap in the open conformation (as in PDB files 1UBP, 2UBP, and 4UBP) and closed conformation (as in 3UBP).

### Grid computation

The program GRID 4.0 [21, 22] was used to calculate the ligand-receptor interaction energy as described by Eq. 1:

$$E = \sum_{i=1}^{\text{lig}} \sum_{j=1}^{\text{rec}} \left[ \frac{A_{ij}}{r_{ij}^{12}} - \frac{B_{ij}}{r_{ij}^{6}} + 332 \frac{q_i q_j}{D r_{ij}} \right] \tag{1}$$

In this equation, the atoms of the ligands are indicated as $i$, and those of the receptor as $j$. The first two terms of this equation describe a Lennard-Jones 12-6 potential, while the last term is the Coulomb potential. $D$ is the dielectric value modelled as a function of the distance ($D$=$Nr$), and 332 is a factor to convert the electrostatic energy in kcal/mol. The van der Waals repulsive and attractive parameters ($A_{ij}$ and $B_{ij}$, respectively) are approximated as described in Eq. 2:

$$\begin{aligned} A_{ij} &= \sqrt{A_{ii}} \cdot \sqrt{A_{jj}} \\ B_{ij} &= \sqrt{B_{ii}} \cdot \sqrt{B_{jj}} \end{aligned} \tag{2}$$

The single-atom type parameters ($A_{ii}$, $A_{jj}$, $B_{ii}$, and $B_{jj}$) are calculated as in Eq. 3, in which $R$ is the atomic van der Waals radius, and $\varepsilon$ is the well depth:

$$\begin{aligned} A &= \epsilon (2R)^{12} \\ B &= 2\epsilon (2R)^{6} \end{aligned} \tag{3}$$

Using this approximation, the overall ligand-receptor interaction energy can be written as in Eq. 4:

$$E = \sum_{i=1}^{\text{lig}} \left[ \sqrt{A_{ii}} \sum_{j=1}^{\text{rec}} \frac{\sqrt{A_{jj}}}{r_{ij}^{12}} - \sqrt{B_{ii}} \sum_{j=1}^{\text{rec}} \frac{\sqrt{B_{jj}}}{r_{ij}^{6}} + 332 q_i \sum_{j=1}^{\text{rec}} \frac{q_j}{D r_{ij}} \right] \tag{4}$$

It is then possible to consider three values for every grid point ($k$), $A_{\text{rec}}$, $B_{\text{rec}}$, and $Q_{\text{rec}}$ (Eq. 5), each a sum over receptor atoms that are within a user-defined cut-off distance of the point:

$$\begin{aligned} A_{\text{rec}} &= \sum_{j=1}^{\text{rec}} \frac{\sqrt{A_{jj}}}{r_{kj}^{12}} \\ B_{\text{rec}} &= \sum_{j=1}^{\text{rec}} \frac{\sqrt{B_{jj}}}{r_{kj}^{6}} \\ Q_{\text{rec}} &= 332 \frac{q_j}{D r_{kj}} \end{aligned} \tag{5}$$

These three values are finally multiplied by the appropriate ligand values to give the interaction energy as in Eq. 6:

$$E = \sum_{i=1}^{\text{lig}} \left[ A_{\text{rec}} \sqrt{A_{ii}} - B_{\text{rec}} \sqrt{B_{ii}} + q_i Q_{\text{rec}} \right] \tag{6}$$

For the present calculation, a box (8 Å edge) centered between the Ni atoms was considered for the grid calculation (points spacing of 0.3 Å), the cut-off distance for the interaction energy was 12 Å, and the dielectric factor was $N$=4.

All the receptor parameters used by GRID (atomic van der Waals radii, well depths, and partial charges) were those included in the all-atom AMBER 5 (Cornell) force field [28]. Histidine residues were considered neutral, while the Ni-bound Asp$^{\alpha 363}$ was considered deprotonated. Partial charges over the non-standard residues (carbamylated lysine and Cys-S-S-BME)

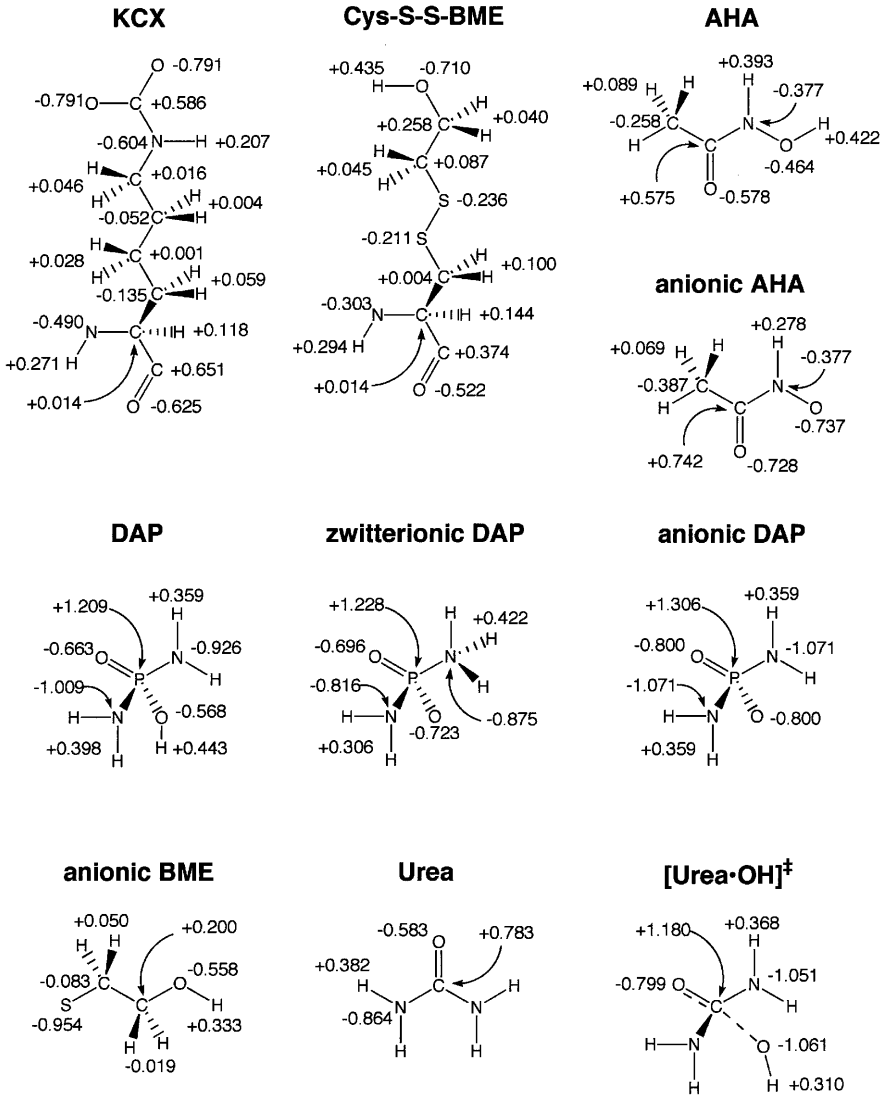


**Fig. 3** Partial atomic charges calculated using the RESP procedure over non-standard amino acids found in the reaction site (carbamylated lysine and Cys-S-S-BME), inhibitors, urea, and reaction transition state

were calculated using GAUSSIAN 94 [29] at the HF/6-31G(d) level, and refined with RESP (restrained electrostatic potential) [30, 31], according to the procedure used to assign atomic charges in AMBER 5 (Fig. 3). The radius (1.170 Å), charge (2+ ), and van der Waals well depth (0.100 kcal/mol) for Ni were taken as the DOCK default values for closed-shell ions. Different values yielded higher RMSD between calculated and experimental structures.

## Ligands characterization

The geometry of water, hydroxide, and urea, as well as the catalytic transition state, were calculated using ab initio methods (GAUSSIAN 94) based on the DFT [16, 17] at the B3LYP/6-31+G(d) level. In the case of urea, the optimized geometry was in excellent agreement with the crystallographic data (Table 2) [32]. The geometries of BME, AHA, and DAP were taken from the available PDB files 1UBP, 4UBP, and 3UBP, respectively. Hydrogen positions, not available from the crystal structures, were calculated using the ab initio and DFT methods described above. Table 2 reports the calculated geometric parameters for urea and the reaction transition state.

The atomic partial charges were calculated at the HF/6-31G(d) level (GAUSSIAN 94) and fitted using the RESP pro-

**Table 2** B3LYP/6-31+G(d) optimized geometry of urea and of the catalytic transition state. All distances are in Å and angles are in degrees

| Urea | B3LYP/6-31+G(d) | Exp[a] | $[Urea.OH]^-$ transition state | B3LYP/6-31+G(d) |
|---|---|---|---|---|
| C-O | 1.226 | 1.200 | $C\text{-}O_R$[d] | 1.959 |
| C-N | 1.383 | 1.370 | C-O | 1.246 |
| $N\text{-}H_T$[b] | 1.009 | 0.999 | $O_R\text{-}H_R$[d] | 0.969 |
| $N\text{-}H_C$[c] | 1.011 | 0.998 | C-N | 1.449 |
| N-C-N | 115.2 | 114.6 | $N\text{-}H_T$ | 1.019 |
| $H_T\text{-}N\text{-}C$ | 121.3 | 118.7 | $N\text{-}H_C$ | 1.015 |
| $H_C\text{-}N\text{-}C$ | 114.7 | 114.1 | $O\text{-}C\text{-}O_R$ | 109.4 |
| O-C-N | 122.3 | 122.7 | O-C-N | 118.8 |
| | | | N-C-N | 111.3 |

[a] See [32]
[b] $H_T$: hydrogen in *trans* position, referred to urea carbonyl group
[c] $H_C$: hydrogen in *cis* position, referred to urea carbonyl group
[d] $O_R$ and $H_R$: oxygen and hydrogen from reacting hydroxide

cedure, consistent with the procedure used to calculate charges on the receptor atoms. Figure 3 shows the results of such calculations for a representative set of ligands.

The present work makes the assumption that the molecular geometry and charge distribution calculated with such procedure (in the gas phase) is comparable to the geometry of the same molecule in solution or in the enzyme active site. Even though this approximation does not include other effects, such as those derived by the presence of solvent molecules, the calculated structures of docked ligands correspond largely to the structures of urease complexes determined by X-ray crystallography (see below). Therefore it was considered acceptable for the purposes of the present work.

### Docking

Molecular recognition was performed using DOCK 4.0.1 [18, 23]. This program performs an orientation search by comparing the distances between the spheres, calculated using SPHGEN, with the distances of the atoms of a rigid molecule (the all-atom model was used here). If $d_{ij}$ is the distance between atoms $i$ and $j$ of the ligand, and $d_{kl}$ is the distance between sphere centers $k$ and $l$, the orientation is accepted when:

$$|d_{ij} - d_{kl}| lt; \epsilon \tag{7}$$

where $\varepsilon$ represents an arbitrary small convergence limit (a value of 0.3 Å was used here for all calculations). In this way, the program generates a large number of clusters containing pairs of atoms/spheres for which Eq. 7 is true. It is also possible to dock a flexible molecule using a procedure called "fragmentation". With this option, the ligand molecule is divided into different fragments characterized by the absence of conformational freedom. The first orientation search is performed on a rigid fragment called the "anchor". When the anchor has been docked, the program attaches the second fragment on it, performing a conformational search on a set of possible torsion angles defined by the bond features. This procedure is repeated until the molecule is fully reconstructed. The conformation search follows a tree search: the program studies first the orientation of the fragment near to the anchor, pruning the orientations that give high energies or contact violations with the spheres of the receptor, and then docks the following fragments. The final orientations and conformations are refined using a rigid-body energy minimization, and are finally listed in order of increasing interaction energy (decreasing score), which includes both inter- and intramolecular van der Waals and electrostatic factors.

If the crystallographic structure of the ligand inside the reaction site is available, it is possible to check the reliability of the simulation by computing the root mean square deviation (RMSD) from the experimental data (Eq. 8):

$$\mathrm{RMSD} = \sqrt{\frac{\sum_{i,j=1}^{N} \left(\mathbf{x}_i - \mathbf{x}_j\right)^2}{N}} \tag{8}$$

where $\mathbf{x}_i$ is the coordinate vector of the simulated structure, $\mathbf{x}_j$ is the coordinate vector of the experimental structure, and $N$ is the number of atoms. On the other hand, if the structure is not available, the RMSD* parameter is defined here as the deviation (calculated according to Eq. 8) of each orientation from the structure having the lowest energy.

## Results

The calculations performed and described in the present report can be divided into two sequential sections: (1) optimization of the docking parameters by comparing the experimental and calculated best structures of BME-, AHA-, and DAP-inhibited BPU, and (2) utilization of these parameters to dock the substrate and the catalytic transition state in order to probe the two proposed catalytic mechanisms for urea hydrolysis.

### Docking of BME

Figure 4A (top panel) shows a plot of RMSD versus energy score for the docking of BME into the active site of BME-inhibited BPU (PDB code 1UBP), characterized by the flap in the open conformation. All accepted solutions constitute a family of structures featuring the thiolate sulfur atom of the inhibitor in a Ni-bridging position, while the rest of the inhibitor assumes different conformations, suggesting a relatively high flexibility of the ligand tail within the active site. The calculated lowest energy structure (Fig. 4A, bottom panel) differs significantly from the crystallographic result (compare with Fig. 2A). The sulfur atom is found to bridge the two Ni ions as observed in 1UBP, but the terminal OH group does not chelate Ni(1), preferring instead to form an H-bond with the carbonyl oxygen of $Ala^{\alpha 170}$. This calculation was performed without considering the second molecule of BME, found to make a disulfide bond with $Cys^{\alpha 322}$ in the X-ray structure (see Fig. 2A).

When the non-standard amino acid $Cys^{\alpha 322}$-S-S-BME was included in the receptor structure, a different distribution of RMSD versus energy score was obtained (Fig. 4B, top panel). The best 12 calculated structures constitute a conformationally homogenous ensemble. The lowest energy simulation (Fig. 4B, bottom panel) shows a BME molecule in a bridging-chelating Ni-binding mode very similar to the experimentally determined structure (RMSD=0.2 Å). This structure further shows the OH proton of BME making an H-bond with the carbonyl oxygen of $Gly^{\alpha 280}$, as also suggested by the crystal structure [10].

If the BME docking simulation is performed using an active site cavity characterized by a closed conformation for the flap (as in PDB code 3UBP), the plot of RMSD* versus energy score shown in Fig. 4C (top panel) is obtained. The values for the calculated energies of the docked structures are much higher than those observed when an open flap is considered (see Fig. 4A and B, top panels). The calculated best 16 structures constitute a conformationally homogeneous family, characterized by a thiolate sulfur atom consistently bridging the two Ni ions, while the tail of the molecule is directed away from the metal ions, toward the active site opening. The lowest energy structure, shown in Fig. 4C, reveals that the inhibitor bridges the two Ni ions with the anionic sulfur atom. However, its terminal OH group does not chelate Ni(1), rather making a charge-assisted H-bond with $Arg^{\alpha 339}$ and an H-bond with $His^{\alpha 323}$ (not shown in Fig. 4C for the

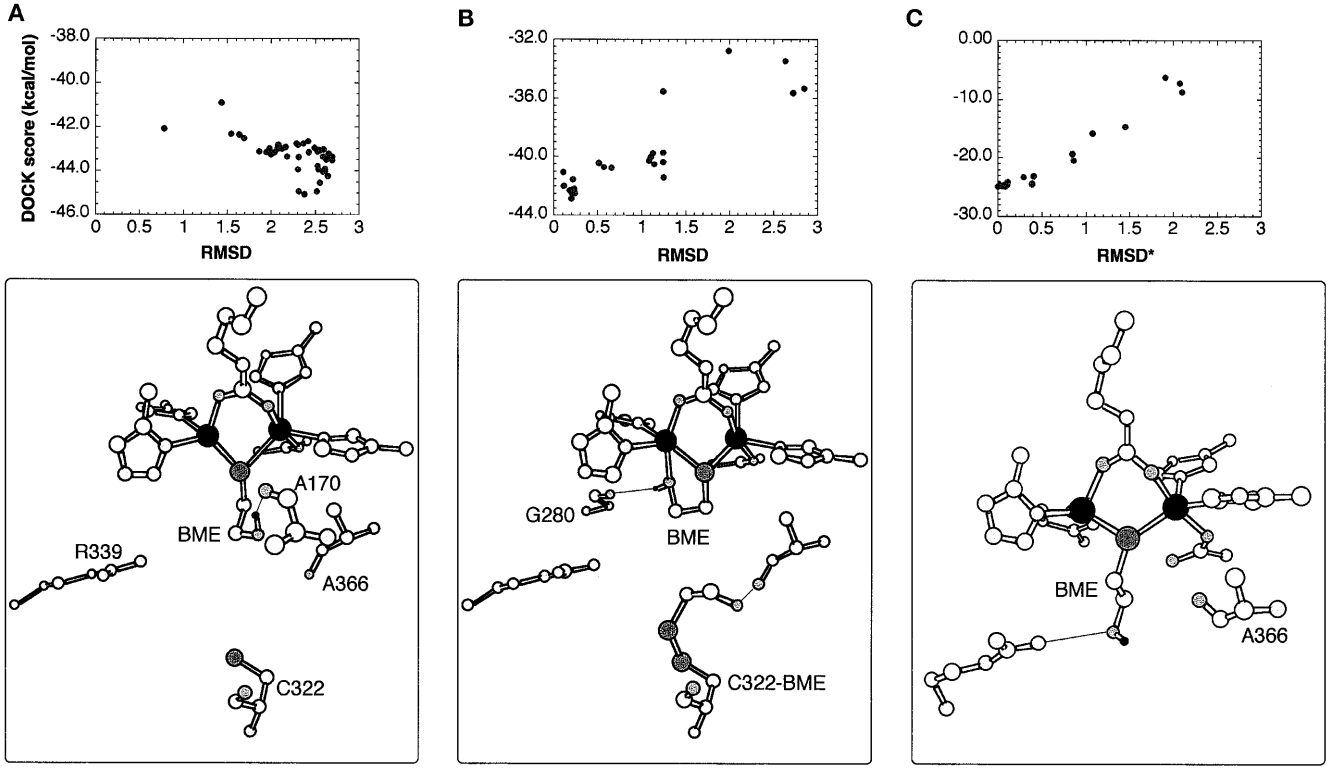


**Fig. 4A–C** BME docking simulations. RMSD versus energy score (*top panels*) and best score structure (*bottom panels*). **A** Dock of BME molecule in the open flap active site devoid of Cys-S-S-BME disulfide; **B** dock of BME molecule in the open flap active site containing the Cys-S-S-BME disulfide; **C** dock of BME molecule in the closed flap active site devoid of Cys-S-S-BME disulfide (color scheme: nickel, *black*; carbon, *white*; nitrogen, *light grey*; oxygen, *grey*; sulfur, *dark grey*; hydrogen, *black*). H-bonds are shown as *thin lines*

sake of clarity). All other structures feature the inhibitor thiolate atom in the Ni-bridging position and different conformations for the rest of the molecule.

## Docking of AHA

The simulation of neutral AHA inserted into the reaction site of AHA-inhibited BPU (PDB code 4UBP) yields a plot of RMSD versus energy score (Fig. 5A, top panel) featuring the presence of a single family of six structures characterized by a very consistent position of all inhibitor atoms. The structure having the best score, shown in Fig. 5A (bottom panel), reveals a calculated position of AHA that is quite different from the experimental data (Fig. 2B). The calculation suggests that the inhibitor in the neutral form would bridge the two Ni ions using the hydroxamic oxygen atom, consistent with the crystallographic observation. However, the carbonyl group chelates Ni(2) rather than Ni(1), therefore imposing a completely different coordination geometry to the metal ions (pseudo-tetrahedral versus trigonal bipyramidal for Ni(1), and pseudo-octahedral versus trigonal bipyramidal for Ni(2))[1]. In addition, the bridging Ni-O distances (2.1 and 2.4 Å) are larger than those observed in the crystal structure (1.9 and 2.0 Å).

Docking the anionic form of AHA into the same reaction site yields several structures having a much lower energy than for neutral AHA (see Fig. 5B, top panel). A well-defined single family of structures can be identified, and the best score structure, shown in Fig. 5B, displays features very similar to those observed experimentally (compare with Fig. 2B). The H-bonding network stabilizing the inhibitor in the active site is well reproduced by the simulation.

It has been proposed that AHA binds as the neutral form to the active site of BPU in an initial weak complex featuring the AHA carbonyl group bound to Ni(1) and the AHA-OH group H-bonded to the bridging hydroxide [11]. In order to test this proposal, a calculation was carried out by docking a molecule of neutral AHA into the active site of native BPU (PDB code 2UBP) from which all water molecules, except for the bridging hydroxide, had been removed. The

[1] The present work makes the assumption that, even though the docking calculation does not consider bond stabilization energies or orbital rearrangements, a coordination bond is formed when the distance between a donor atom and a metal ion is analogous to the usual bond distances observed in coordination compounds. This certainly represents a simplification, albeit useful in order to better describe the calculated structures

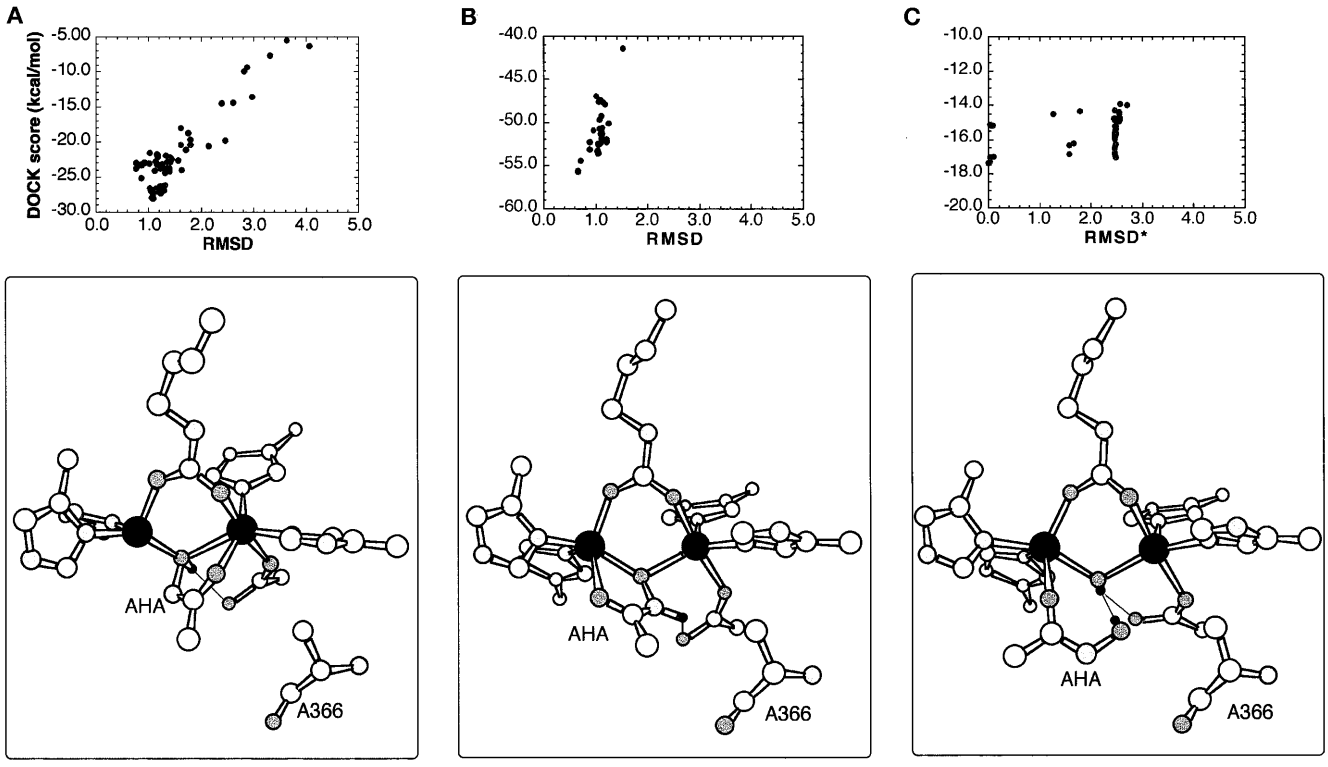


**Fig. 5A–C** AHA docking simulations. RMSD versus energy score (*top panels*) and best score simulation (*bottom panels*). **A** Dock of neutral AHA in the open flap active site; **B** dock of anionic AHA in the open flap active site; **C** dock of neutral AHA in the open flap reaction site containing the bridged hydroxide found in the experimental native BPU structure. The color scheme is identical to that used in Fig. 4. H-bonds are shown as *thin lines*

best score structure, shown in Fig. 5C, fully supports the above proposal, showing a molecule of AHA forming a strong H-bond between the terminal OH and the Ni-bridging hydroxide, while another H-bond is formed between $His^{\alpha 219}$ N$\varepsilon$H and the Ni(1)-bound AHA carbonyl group.

## Docking of DAP

Figure 6 shows the results of simulations performed using DAP in three possible protonation states: neutral, zwitterionic, and anionic. In this case, the structure of the receptor active site found in DAP-inhibited BPU (PDB code 3UBP), featuring a closed flap, was used.

Figure 6A (top panel), showing the docking results for neutral DAP, displays three low-energy families. The family having the lowest energy overall is constituted by six structures, the most stable one represented in Fig. 6A (bottom panel). In this structure, the overall position of DAP is in good agreement with the crystallographic results (see Fig. 2C), but features the DAP hydroxide moiety H-bonded to $Gly^{\alpha 280}$ (at 2.6 Å) instead of bridging the nickel ions, as proposed for the X-ray structure [8]. This is the reason for the relatively high RMSD (2.3 Å) for this structure. The Ni-ligand distances (Ni-$O_B$=2.2 Å, Ni-O/N=2.3 Å) are very similar to those found in the X-ray structure (2.2–2.3 Å). A strong H-bond network, holding in place the inhibitor molecule, is also observed (Fig. 6A, bottom panel). The additional two low-energy families (RMSD ca. 0.6 and 1.8 Å) observed in Fig. 6A (top panel) feature the same overall position of the inhibitor, but the positions of some atoms are swapped (i.e. the bridging atom is the hydroxide or the amide moiety, respectively). It is noteworthy that these three structural ensembles are separated by only few kcal/mol.

Simulations carried out using DAP in the zwitterionic protonation state produce a predominant family of docked structures (Fig. 6B, top panel). The lowest energy structure, shown in Fig. 6B (bottom panel), reveals that one oxygen atom bridges the Ni ions (Ni-$O_B$ distances=2.1–2.2 Å) and another oxygen atom binds to Ni(1) (at 2.3 Å). In these structures the DAP-$NH_2$ group is bound to Ni(2) (at 2.3 Å), while the DAP-$NH_3$ group points away from the Ni ions and makes two H-bonds with $His^{\alpha 323}$ N$\varepsilon$, and $Ala^{\alpha 366}$ O. One H-atom is positioned between $Gly^{\alpha 280}$ O (at 2.9 Å) and $Asp^{\alpha 363}$ O$\delta$2 (at 2.3 Å). The docking energy score of zwitterionic DAP is higher (i.e. less stable) than in the case of neutral DAP.

The last simulation was carried out using anionic DAP. Figure 6C (top panel) shows that, in this case,

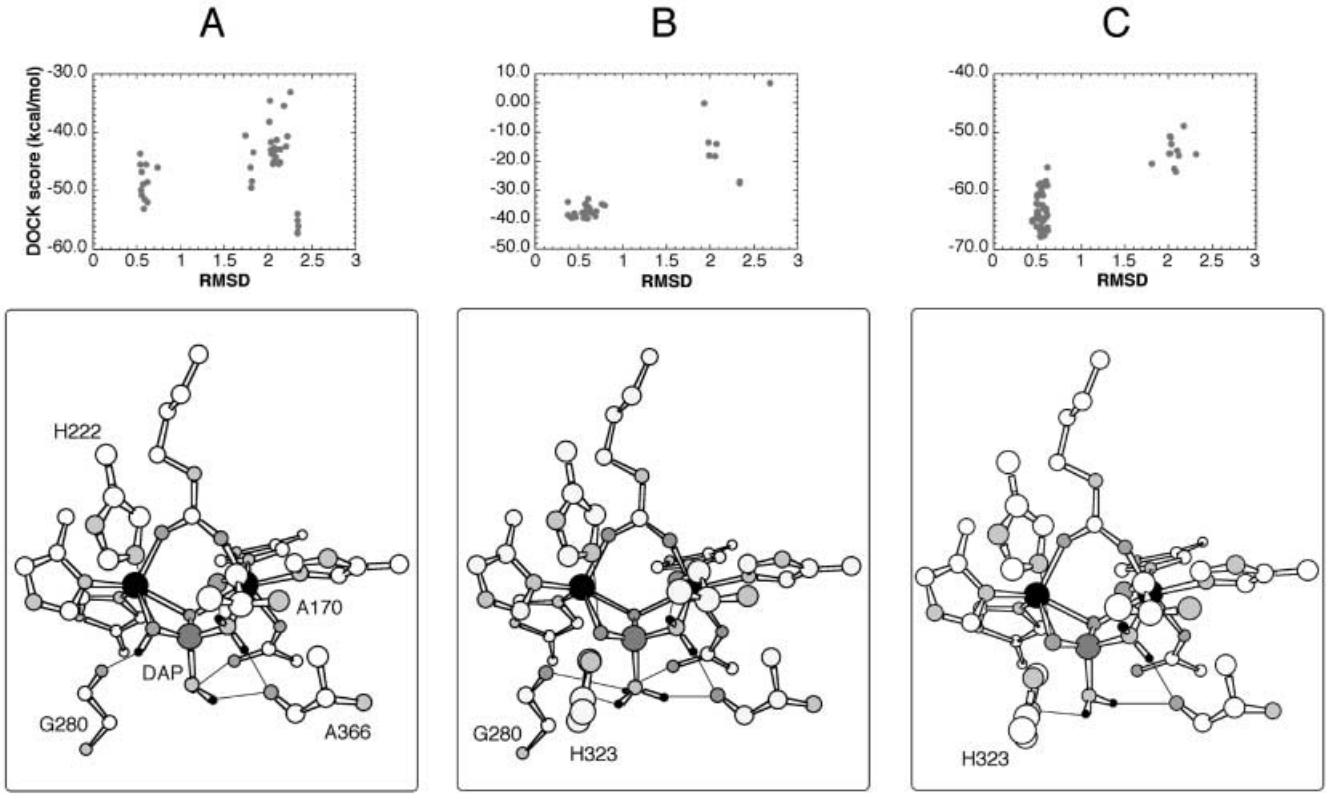


**Fig. 6A–C** DAP docking simulations. RMSD versus energy score (*top panels*) and best score simulation (*bottom panels*). The simulations refer to the case of neutral (**A**), zwitterionic (**B**), and anionic (**C**) DAP in the closed flap active site (color scheme: nickel, *black*; carbon, *white*; nitrogen, *light grey*; oxygen, *grey*; phosphorus, *dark grey*; hydrogen, *black*). H-bonds are shown as *thin lines*

there is one largely predominant family of docked structures featuring a very small RMSD (0.5 Å) and the lowest energy score observed for this set of simulations (–68 kcal/mol). The corresponding lowest energy structure (Fig. 6C, bottom panel) features atomic positions remarkably similar to the crystallographic structure (Ni-$O_B$=2.2 Å, Ni-O/N=2.3–2.4 Å). These results suggest the presence of anionic DAP in the inhibited urease reaction site, while the analysis of the X-ray structure had previously suggested the presence of the neutral form of the inhibitor [8].

## Urease reaction mechanism; urea binding

Following the reaction path models presented in Scheme 1, and adopting the same parameters used to successfully simulate the structure of urease complexed with inhibitors as described above, a set of calculations was performed in order to explore two key steps of the enzymatic reaction mechanism of urea hydrolysis, that is (1) the urea binding and (2) the nucleophilic attack by a hydroxide molecule. The docking calculations enabled us to take "snapshots" of the reaction profile by looking at the conformations adopted by the ligands (substrate and transition state) in the active site.

Figure 7 shows the results of calculations involving the interaction of urea with the urease active site featuring the flap in the open conformation (as in 2UBP), presumably the first step of the reaction. The calculations entailed (1) an active site featuring the Ni-bridging hydroxide but completely devoid of water molecules (as proposed in mechanism A of Scheme 1) or (2) a site containing both the bridging and a Ni(2)-bound terminal hydroxide (as proposed in mechanism B of Scheme 1). In the second case, the position of the terminal hydroxide was taken as that of the crystallographically determined Ni(2)-bound water molecule in 2UBP. The results of the calculations are shown in Fig. 7A and B, respectively.

Figure 7A (top panel) reveals a family of structures featuring very similar atomic positions, while Fig. 7A (bottom panel) shows the corresponding lowest energy structure. The latter is characterized by the urea O atom at 2.6 Å from Ni(1), H-bonded to $His^{\alpha 222}$. The urea C atom is in a favorable position for a nucleophilic attack by the bridging hydroxide ($O_B$-C=3.2 Å, Ni-$O_B$-C angles=102.3°/126.0°). On the other hand, Fig. 7B (top panel) reveals the presence of a family of simulated structures more scattered but more stable (lower energy) than that observed in Fig. 7A. The lowest energy structure, representative of the first 25 best structures (Fig. 7B, bottom panel), reveals the

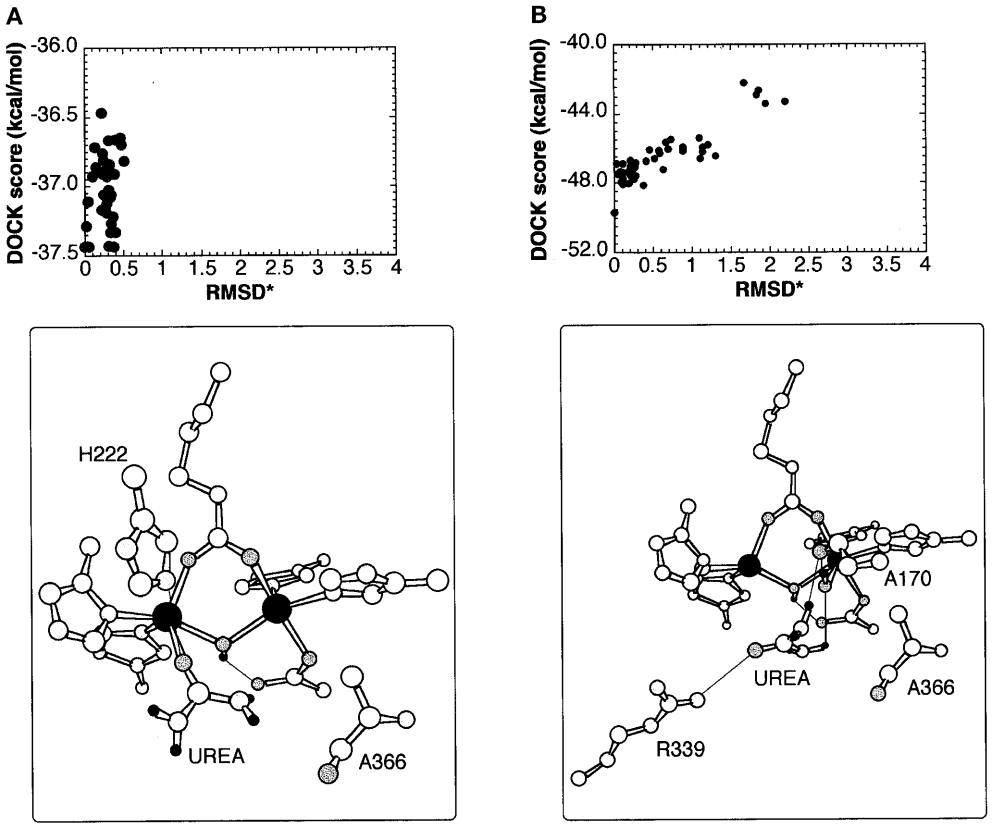


**Fig. 7A, B** Urea docking simulations obtained using the open flap BPU conformation as receptor. RMSD* versus energy score (*top panels*) and best score simulation (*bottom panels*). **A** Urea docked to the active site containing the Ni-bound hydroxide ion; **B** urea docked to the active site containing both the bridging and the Ni(2) terminally bound hydroxide. The color scheme is identical to that used in Fig. 4. H-bonds are shown as *thin lines*

presence of a urea molecule non-coordinated to the metal ions and stabilized by several H-bonds, formed between $Arg^{\alpha 339}$ and the urea O atom, between a urea $NH_2$ group and $Ala^{\alpha 170}$ O, and between the second urea $NH_2$ group and the Ni(2)-bound OH moiety.

Figure 8 shows the results of docking calculations performed as described above for Fig. 7, but now involving the interaction of urea with an active site featuring the flap in the closed conformation (as in 3UBP). When a site containing only the bridging hydroxide is considered (according to mechanism A of Scheme 1) the calculations reveal the absence of a well-defined family of structures, with two isolated low-energy positions for urea (Fig. 8A, top panel). The lowest score structure, representative of the best eight energy scores and shown in Fig. 8A (bottom panel), reveals that urea does not form any coordination bonds with the Ni ions, while its $NH_2$ groups form H-bonds with $His^{\alpha 323}$ N$\varepsilon$ and $Asp^{\alpha 363}$ O$\delta$2. On the other hand, the docking of urea to a site containing a Ni(2)-bound hydroxide (following mechanism B of Scheme 1) produces several structures, with lower energies than in the previous case (Fig. 8B, top panel) and not constituting a homogenous family. The lowest energy structure (Fig. 8B, bottom panel), representative of the best 10 scores, reveals a molecule of urea involved in a strong H-bonding network with both bridging and terminal hydroxide ions, as well as with $Gly^{\alpha 280}$ O and $Ala^{\alpha 366}$ O, but, again, the absence of coordination bonds between urea and the Ni ions.

Urease reaction mechanism; transition state binding

The second snapshot of the mechanism involved docking the reaction transition state according to the two reaction models proposed in Scheme 1. The first set of calculations (Fig. 9) considered an active site flap in the open conformation (as in 2UBP). The transition state was docked in the active site devoid of all water/hydroxide molecules (Fig. 9A) as well as containing the nickel-bridging hydroxide (Fig. 9B), in order to probe mechanisms A and B in Scheme 1. In the first case, a highly populated low-energy family was determined (Fig. 9A, top panel), and the best score structure is shown in Fig. 9A (bottom left panel). In this structure, the reacting nucleophilic hydroxide is placed between the nickel ions, with Ni-$O_B$ distances of 2.1 and 2.2 Å with Ni(1) and Ni(2), respectively. Ni(1) interacts with a transition state N atom at 2.4 Å, while the distance between Ni(2) and the second O atom of the transition state is 3.2 Å. The hydrogen atom located on the hydroxide group on the transition state forms an H-bond with $Ala^{\alpha 170}$ O, while the two amino groups in the transition state are H-bound to $Gly^{\alpha 280}$ O and $Asp^{\alpha 363}$ O$\delta$2, respectively.

In the case of the transition state docked to an active site containing the bridging hydroxide, the results are ambiguous. Figure 9B (top panel) shows two structural families. The structure with the lowest energy, shown in the central-bottom panel of Fig. 9B, features the transition state bound to Ni(1) with an

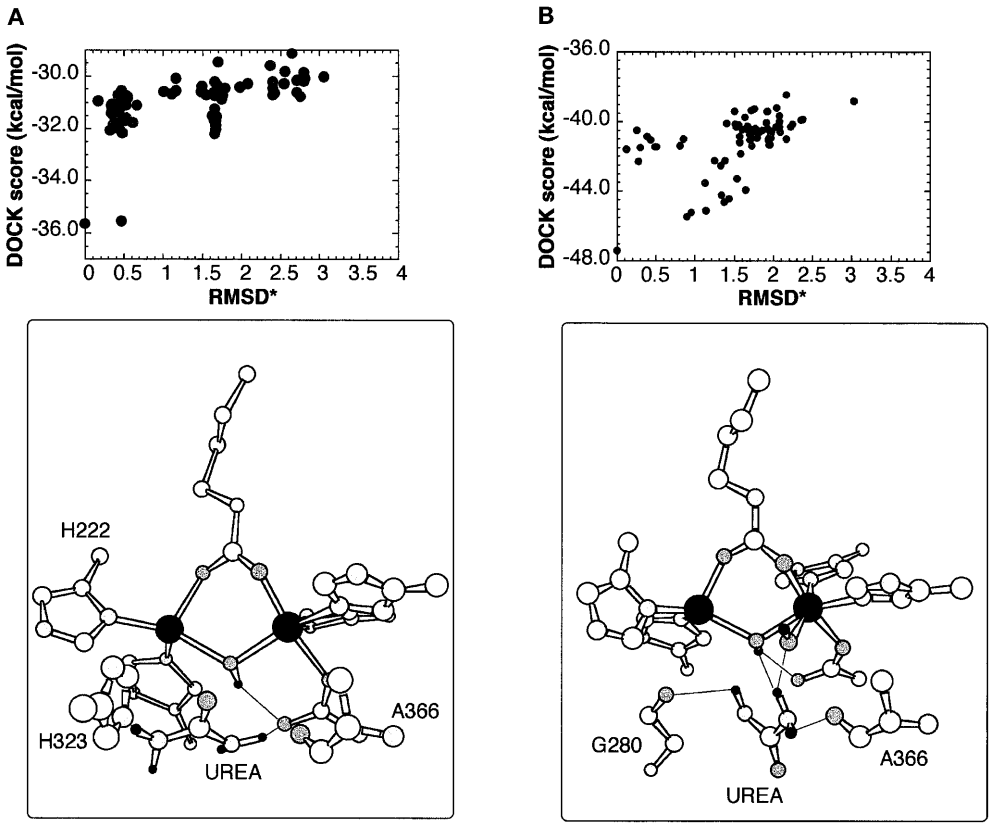


**Fig. 8A, B** Urea docking simulations obtained using the closed flap BPU conformation as receptor. RMSD* versus energy score (*top panels*) and best score simulation (*bottom panels*). **A** Urea docked to the active site containing the Ni-bound hydroxide ion; **B** urea docked to the active site containing both the bridging and the Ni(2) terminally bound hydroxide. The color scheme is identical to that used in Fig. 4. H-bonds are shown as *thin lines*

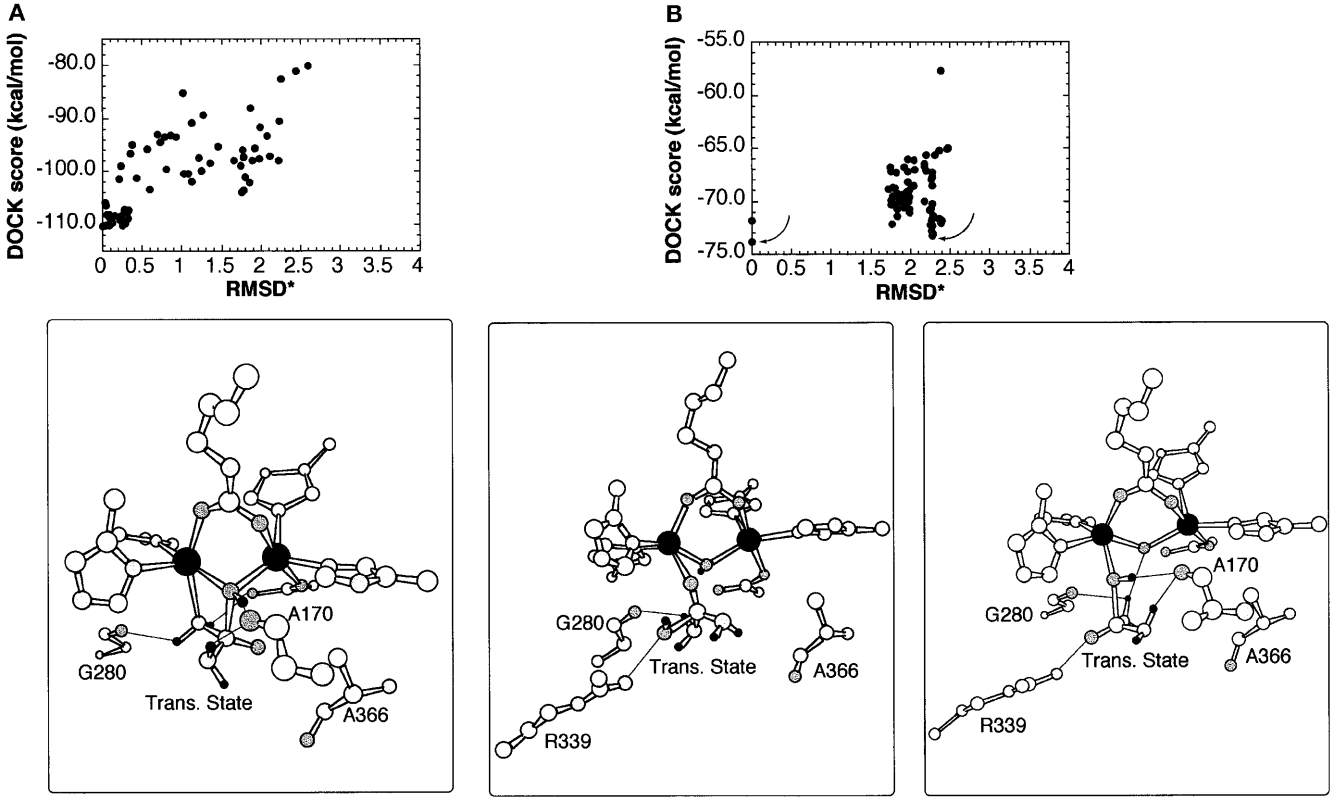


**Fig. 9A, B** Transition state docking simulations using the open flap BPU conformation as receptor. RMSD* versus energy score (*top panels*) and best score simulation (*bottom panels*). **A** Transition state docked to the active site devoid of any water/hydroxide Ni ligands; **B** transition state docked to the active site containing the bridged hydroxide ion, and second-best score. The color scheme is identical to that used in Fig. 4. H-bonds are shown as *thin lines*

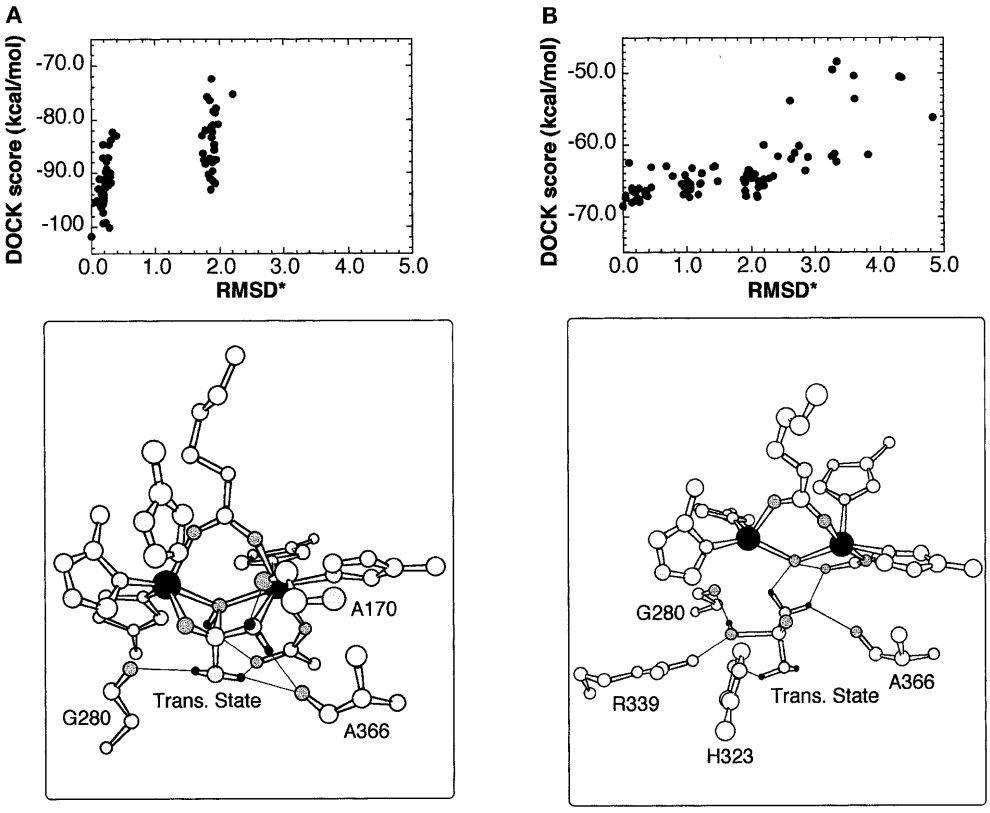


**Fig. 10A, B** Transition state docking simulations using the closed flap BPU conformation as receptor. RMSD* versus energy score (*top panels*) and best score simulation (*bottom panels*). **A** Transition state docked to the active site devoid of any water/hydroxide Ni ligands; **B** transition state docked to the active site containing the bridged hydroxide ion. The color scheme is identical to that used in Fig. 4. H-bonds are shown as *thin lines*

oxygen atom at 2.5 Å, while the reacting hydroxide, H-bound to $Arg^{\alpha 339}$, points toward a region of the reaction site far from the metal ions. The second best score structure (bottom right panel of Fig. 9B) belongs to a different, more populated ensemble, and is characterized by a reacting hydroxide bound to Ni(1) at a distance of 2.1 Å, while the urea oxygen atom forms an H-bond with $Arg^{\alpha 339}$.

An additional set of calculations was performed by docking the transition state to an active site featuring the flap in the closed conformation (as in 3UBP). The results are shown in Fig. 10. Only two well-resolved families are determined in the case of a transition state docked to an active site devoid of water/hydroxide molecules, according to mechanism A of Scheme 1 (Fig. 10A, top panel). The best score structure (Fig. 10A, bottom panel) is representative of the best 17 structures and reveals a transition state positioned in the active site with the nucleophilic OH group symmetrically bridging the Ni ions (Ni-$O_B$=2.1 Å). The Ni ions coordination shells are completed by the anionic oxygen (Ni(1)-O=2.3 Å) and one $NH_2$ group (Ni(2)-N=2.5 Å). This structure features atomic positions largely coincident with those determined in the crystal structure of DAP-inhibited urease (see Fig. 2C). Also, the H-bonding network is essentially identical to that found stabilizing the DAP molecule in inhibited urease (see Fig. 2C). Therefore, this result supports the hypothesis that DAP is a good representative of the transition state of the reaction [8]. The second family of structures observed in the top panel of Fig. 10A differs from the most stable ensemble only because of swapped O and OH groups.

The results of calculations carried out using a receptor active site which includes the bridging hydroxide (according to mechanism B in Scheme 1) are shown in Fig. 10B. In this case the docking energy is ca. 30 kcal/mol higher than in the case of mechanism A, while it is very difficult to identify well-defined structural families. Figure 10B shows the lowest energy structure for this case, representative of the first seven best scores. In this structure, no transition state atom forms any bonds with the nickel ions, preferring to build an H-bonding network with neighbouring residues ($Ala^{\alpha 170}$, $His^{\alpha 222}$, $Gly^{\alpha 280}$, $Asp^{\alpha 363}$, $Arg^{\alpha 339}$, and $Ala^{\alpha 366}$). In this structure, the reacting hydroxide is located closer to Ni(1) (4.2 Å) than to Ni(2) (6.0 Å).

## Discussion

### Inhibitor binding

The procedure devised to perform simulations of known urease-ligand complexes resulted in successfully reproducing the related crystal structures, with the additional caveat that the conformation of the active site flap is critical. In fact, the active site cavities calculated by considering both the open and closed flap conformations reveal a distinct reduction of the volume available for a putative ligand in the

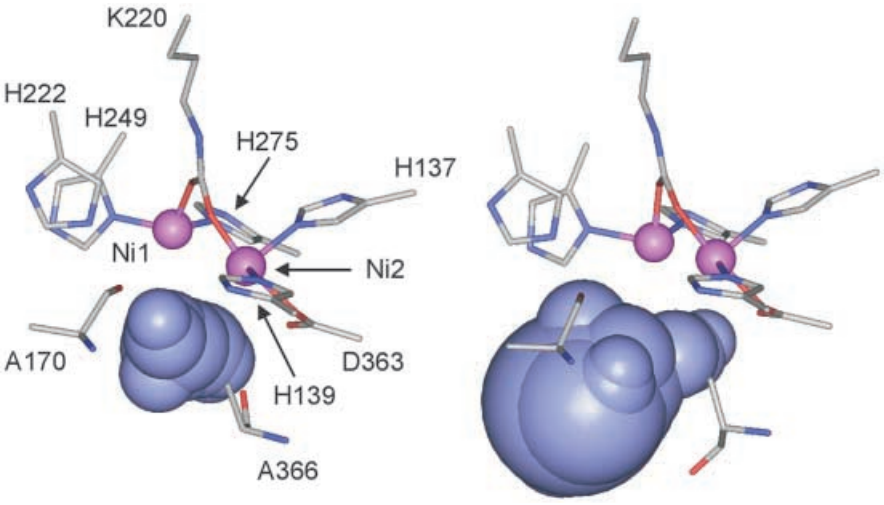


**Fig. 11** Negative image of the reaction site as calculated by the program SPHGEN in the closed (*left panel*) and open (*right panel*) flap conformation. The color scheme is identical to that used in Fig. 2, while the reaction site cavity is shown in *violet*

active site upon flap closure (Fig. 11). Such an observation highlights the critical role of the position of this motif on the catalytic reactivity of urease.

This is clearly the case of BME docking, which suggests that the first incoming inhibitor molecule places the sulfur atom in the bridging position between the two Ni ions, substituting the Ni-bridging hydroxide ion (Fig. 4). In this case, the inhibitor tail would be flexible and free to adopt several conformations in the active site, stabilized by H-bonding interactions with different active site residues. The latter behavior would be independent of the flap conformation (compare Fig. 4A and C, bottom panels), even though the formation of the inhibitor complex would induce a flap opening (as inferred by the lower energy observed in Fig. 4A and C, top panels). The hydroxylated tail adopts the chelate conformation found in the crystal structure only subsequent to the formation of a disulfide bond between a second molecule of BME and a nearby Cys residue (Fig. 4B). The second molecule of BME must therefore significantly modify both the steric and electrostatic environment of the active site. It is important to notice that the Cys-S-S-BME covalent disulfide bond observed in the 1UBP crystal structure could have been formed during the prolonged exposure of the concentrated urease/BME solution to oxygen.

The docking calculations have also provided hints on the protonation state of the inhibitors in the active site, as in the case of both AHA and DAP. In the first case (Fig. 5), the anionic AHA was docked in the active site with significantly lower energy than in the case of the neutral inhibitor. Also, suggestions for the inhibition mechanism by AHA were inferred. In the case of DAP, the best energy simulations suggest that DAP binds in the anionic form to the active site (Fig. 6).

## Analysis of the reaction mechanism

For any plausible enzymatic mechanism for Ni-mediated urea hydrolysis, the atomic positions of the substrate (in this case urea and hydroxide) and transition state should fulfill the three following requirements:

1. Involve Ni-coordination of either urea or the incoming nuclephilic hydroxide in the transition state.
2. Adopt low energy conformations.
3. Be as conserved as possible throughout the catalysis, in order to speed up the reaction.

According to these criteria, the dock of urea in the open flap conformation of urease (Fig. 7) suggests that the first step of the reaction is the formation of a bond between the urea oxygen atom and Ni(1) in the absence of a Ni(2)-bound solvent molecule, with the flap in the open conformation. Closure of the flap (Fig. 8) produces unfavorable steric and electrostatic interactions of the substrate within the active site cavity, regardless of the presence or absence of a Ni(2)-bound solvent molecule. Therefore, flap closure should activate the urea molecule, initially bound as shown in Fig. 7A, for further reactivity, which supposedly entails the nucleophilic attack of an active site hydroxide and the formation of the transition state in the active site. The docking of the transition state in the active site, when the flap is open (Fig. 9) or closed (Fig. 10) reveals that the three requirements outlined above are fulfilled only when the transition state is docked to a closed active site devoid of both bridging and Ni(2)-bound hydroxide. This result strongly supports the reaction mechanism A shown in Scheme 1, involving a nucleophilic attack by the bridging hydroxide, and not by the hydroxide terminally bound to Ni(2). This conclusion is also in agreement with recent kinetic studies on KAU fluoride inhibition [33] and active site variants [34].

In addition to providing theoretical support for mechanism A shown in Scheme 1, the docking calculations suggest a correction to this hypothesis

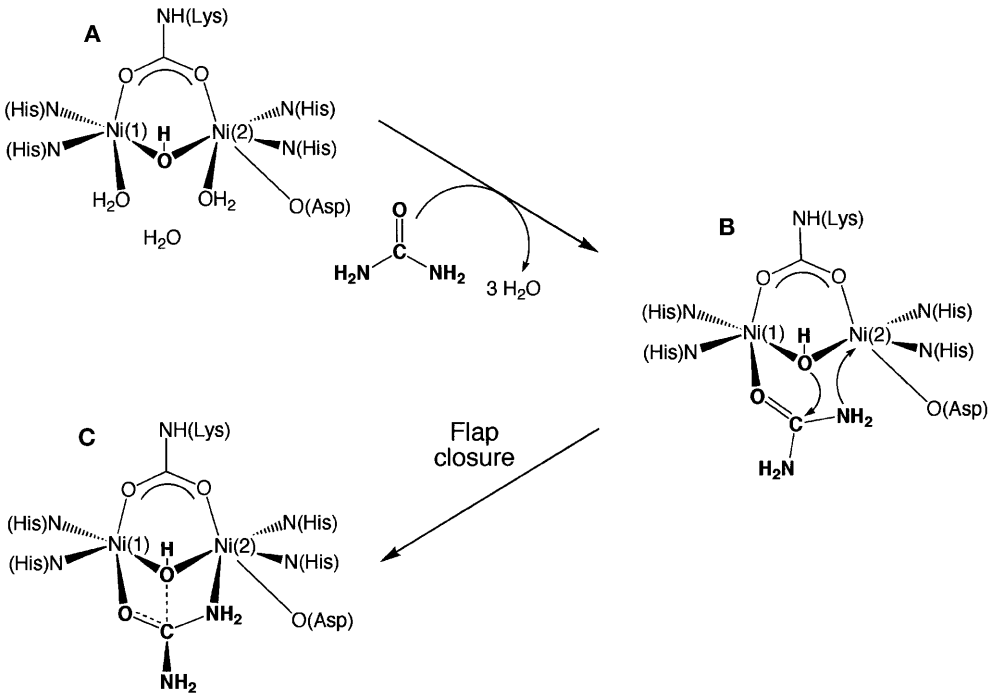


**Scheme 2**

(Scheme 2). Mechanism A in Scheme 1 entails the formation of a coordination bond between the urea $NH_2$ group and Ni(2) upon flap closure prior to the nucleophilic attack of the hydroxide on the urea carbon atom. However, the results reported here suggest the formation of the urea $NH_2$-Ni(2) bond concomitant with, or subsequent to, the formation of the C(urea)-O(bridge) bond upon nucleophilic attack by the bridging hydroxide. The bond between the bridging OH and Ni(1) could be weakened by substrate binding to Ni(1), activating the $OH_B$ for nucleophilic attack. This more concerted (and supposedly faster) mechanism would allow the removal of the urea resonance energy stabilization, at the same time increasing the Lewis base character of the lone pair on the urea nitrogen (as also evident from the DFT calculated charges on urea and the transition state, shown in Fig. 3), favoring the formation of the coordination bond between the urea $NH_2$ group and Ni(2).

## Conclusion

The docking calculations described in the present paper have allowed us to discriminate, on the basis of electrostatic and steric criteria, between the two main proposals present in the literature for urea activation through nucleophilic attack by a hydroxide molecule (see Scheme 1). The calculations have suggested a mechanism involving a concerted formation of (1) a bond between the incoming Ni-bridging hydroxide and the carbon atom of the Ni(1)-bound urea, and (2) a bond between a urea amide nitrogen atom and Ni(2) (see Scheme 2) to yield a stable Ni-bound transition state.

The reported results do not resolve the question of the most viable pathway for the proton transfer to a urea $NH_2$ group. This process has been suggested to involve either (1) a proton transfer from the C-OH moiety of the catalytic intermediate, bridging the two Ni ions through the oxygen [8, 9], or (2) a proton transfer from the protonated catalytically competent $His^{\alpha 323}$ residue, found in the vicinity of the active site [13, 34]. Such questions are currently being addressed in our laboratory using hybrid QM (Car-Parrinello)/MM/MD calculations.

**Acknowledgements** This work was partially supported by grants from the Ministero della Università e della Ricerca Scientifica e Tecnologica (MURST) for the projects "Inorganic structural biology of the biogeochemical cycles of the elements" (to S.C.), "Structural, functional and applicative prospects of proteins from thermophiles" (to R.C.), and by a grant for a target project in Biotechnology from the Italian Centro Nazionale delle Ricerche (CNR) (to R.C.). S.C. thanks S. Benini, S. Mangani, W.R. Rypniewski, and K.S. Wilson for insightful discussions.

## References

1. Hausinger RP (1987) Microbiol Rev 51:22–42
2. Mobley HLT, Hausinger RP (1989) Microbiol Rev 53:85–108
3. Bremner JM Krogmeier MJ (1989) Proc Natl Acad Sci USA 86:8185–8188
4. Bremner JM (1995) Fert Res 42:321–329
5. Collins CM, D'Orazio SEF (1993) Mol Microbiol 9:907–913
6. Mobley HLT, Island MD, Hausinger RP (1995) Microbiol Rev 59:451–480
7. Jabri E, Carr MB, Hausinger RP, Karplus PA (1995) Science 268:998–1004
8. Benini S, Rypniewski WR, Wilson KS, Miletti S, Ciurli S, Mangani S (1999) Struct Fold Des 7:205–216

9. Ciurli S, Benini S, Rypniewski WR, Wilson KS, Miletti S, Mangani S (1999) Coord Chem Rev 190–192:331–355
10. Benini S, Rypniewski WR, Wilson KS, Ciurli S, Mangani S (1998) JBIC 3:268–273
11. Benini S, Rypniewski WR, Wilson KS, Miletti S, Ciurli S, Mangani S (2000) JBIC 5:110–118
12. Andrews RK, Dexter A, Blakeley RL, Zerner B (1986) J Am Chem Soc 108:7124–7125
13. Karplus PA, Pearson MA, Hausinger RP (1997) Acc Chem Res 30:330–337
14. Park I-S, Hausinger RP (1993) J Protein Chem 12:51–56
15. Park I-S, Hausinger RP (1993) Protein Sci 2:1034–1041
16. Hohemberg P, Kohn W (1964) Phys Rev B 136:864–871
17. Kohn W, Sham LJ (1965) Phys Rev A 140:1133–1138
18. Kuntz ID, Blaney JM, Oatley SJ (1982) J Mol Biol 161: 269–288
19. Kuntz ID, Meng EC, Shoichet BK (1994) Acc Chem Res 27:117–123
20. Guiles RD, Sarma S, DiGate RJ, Banville D, Basus VJ, Kuntz ID, Waskell L (1996) Nat Struct Biol 3:333–339
21. Shoichet BK, Bodian DL, Kuntz ID (1992) J Comput Chem 13:380–397
22. Meng EC, Shoichet BK, Kuntz ID (1992) J Comput Chem 13:505–524
23. Ewing TJA, Kuntz ID (1997) J Comput Chem 18:1175–1189
24. Connolly M (1983) J Appl Crystallogr 16:548–558
25. Connolly M (1983) Science 221:709
26. Salo JP, Yliniemela A, Taskinen J (1998) J Chem Inf Comput Sci 38:832–839
27. Shannon RD, Prewitt CT (1976) Acta Crystallogr Sect A 32:751
28. Cornell WD, Cieplak P, Bayly CJ, Gould IR, Merz KM Jr, Ferguson DM, Spellmeyer DC, Fox T, Caldwell JW, Kollman PA (1995) J Am Chem Soc 117:5179–5197
29. Frisch MJ, Trucks GW, Schlegel HB, Gill PMW, Johnson GB, Robb MA, Cheeseman JR, Keith T, Petersson GA, Montgomery JA, Raghavachari K, Al-Laham MA, Zakrzewski VG, Ortiz JV, Foresman JB, Cioslowski J, Stefanov BB, Nanayakkara A, Challacombe M, Peng CY, Ayala PY, Chen W, Wong MW, Andres JL, Replogle ES, Gomperts R, Martin RL, Fox DJ, Binkley JS, Defrees DJ, Baker J, Steward JP, Head-Gordon M, Gonzalez C, Pople JA (1995) Gaussian 94, revision D.3. Gaussian, Pittsburgh
30. Bayly CI, Cieplak P, Cornell WD, Kollman PA (1993) J Phys Chem 97:10269–10280
31. Cornell WD, Cieplak P, Bayly CI, Kollman PA (1993) J Am Chem Soc 115:9620–9631
32. Rousseau B, Van Alsenoy C, Keuleers R, Desseyn HO (1998) J Phys Chem A 102:6540–6548
33. Todd MJ, Hausinger RP (2000) Biochemistry 39:5389–5396
34. Pearson MA, Park IS, Schaller RA, Michel LO, Karplus PA, Hausinger RP (2000) Biochemistry 39:8575–8584
35. Nicholls A, Bharadwaj R, Honig B (1993) Biophys J 64:A166